Biometals (2007) 20:853–867
DOI 10.1007/s10534-006-9079-y

Purification and characterization of rhodobactin: a mixed ligand siderophore from *Rhodococcus rhodochrous* strain OFS

Suraj Dhungana · Ryszard Michalczyk · Hakim Boukhalfa · Joseph G. Lack · Andrew T. Koppisch · Jason M. Fairlee · Mitchell T. Johnson · Christy E. Ruggiero · Seth G. John · Matthew M. Cox · Cindy C. Browder · Jennifer H. Forsythe · Laura A. Vanderberg · Mary P. Neu · Larry E. Hersman

Received: 16 November 2006 / Accepted: 22 December 2006 / Published online: 2 February 2007

Abstract The siderophore produced by *Rhodococcus rhodochrous* strain OFS, rhodobactin, was isolated from iron-deficient cultures and purified by a combination of XAD-7 absorptive/partition resin column and semi-preparative HPLC. The siderophore structure was characterized using 1D and 2D ^{1}H, ^{13}C and ^{15}N NMR techniques (DQFCOSY, TOCSY, NOESY, HSQC and LR-HSQC) and was confirmed using ESI-MS and MS/MS experiments. The structural characterization revealed that the siderophore, rhodobactin, is a mixed ligand hexadentate siderophore with two catecholate and one hydroxamate moieties for iron chelation. We further investigated the effects of Fe concentrations on siderophore production and found that Fe limiting conditions (Fe concentrations from 0.1 μM to 2.0 μM) facilitated siderophore excretion. Our interests lie in the role that siderophores may have in binding metals at mixed contamination sites (containing metals/radionuclides and organics). Given the broad metabolic capacity of this microbe and its Fe scavenging ability, *R. rhodochrous* OFS may have a competitive advantage over other organisms employed in bioremediation.

Keywords *Rhodococcus* · Rhodobactin · Siderophore · Catecholate · Hydroxamate

Electronic Supplementary Material The online version of this article (doi:10.1007/s10534-006-9079-y) contains supplementary material, which is available to authorized users.

S. Dhungana · R. Michalczyk · J. G. Lack · A. T. Koppisch · J. M. Fairlee · J. H. Forsythe · L. A. Vanderberg · L. E. Hersman (✉)
Bioscience, Los Alamos National Laboratory, Mail Stop M888, Los Alamos, NM 87545, USA
e-mail: hersman@lanl.gov

R. Michalczyk
URL:

H. Boukhalfa · M. T. Johnson · C. E. Ruggiero · S. G. John · M. M. Cox · L. A. Vanderberg · M. P. Neu
Chemistry Divisions, Los Alamos National Laboratory, Mail stop J514, Los Alamos, NM 87545, USA

C. C. Browder
Department of Chemistry, Fort Lewis College, 1000 Rim Dr., Durango, CO 81301, USA

S. Dhungana
National Institute of Environmental Health Sciences (NIEHS), 111 T W Alexander Drive, RTP, NC 27709, USA

Introduction

Iron (Fe) is a biologically important nutrient essential for the growth of almost all living organisms. Although Fe is the fourth most abundant element on Earth, its bioavailability is limited severely due to the stability and low solubility of its oxides under aqueous aerobic conditions at biological pH (Crichton 2001; Schwertmann 1991). In fact, the concentration of total dissolved Fe ($Fe^{3+}_{(aq)}$+ $Fe(OH)^{2+}_{(aq)}$ + $Fe(OH)^{+}_{2\ (aq)}$), at pH 7.4 and in the absence of chelators, is $\leq 10^{-10}$ M (Boukhalfa and Crumbliss 2002; Chipperfield and Ratledge 2000), which is nearly 4 orders of magnitude less than is generally required for bacterial growth (Guerinot 1994; Neilands 1995). In response, microorganisms secrete low molecular weight organic chelators called siderophores, which aid in the acquisition and transmembrane transport of Fe by the microbial cell (Albrecht-Gary and Crumbliss 1998; Boukhalfa and Crumbliss 2002; Raymond and Telford 1995). In general, siderophores are classified based on their metal-chelating functionalities, either hydroxamates or catecholates; however, more recently siderophores with new and unusual functional groups, including α-hydroxy carboxylic acid (Albrecht-Gary and Crumbliss 1998; Boukhalfa et al. 2006; Stintzi and Raymond 2002; Winkelmann 1991) and β-hydroxyhistidine, (Dhungana et al. 2003; Dong and Miller 2002; Hancock et al. 1993; Sharman et al. 1995) have been identified to participate in the coordination of iron.

The catecholate class of siderophores generally consists of 2,3-dihydroxybenzoic acid (DHB) moieties for Fe coordination. An exception is petrobactin, which has a unique 3,4-dihydroxybenzoic acid moiety (Barbeau et al. 2002; Koppisch et al. 2005). For catecholate siderophores the DHB moieties often are conjugated to amino acids (Barghouthi et al. 1989; Winkelmann 1991), diamine units such as norspermidine (Yamamoto et al. 1993), or diaminobutane (Page and Vontigerstrom 1988). These siderophores range in complexity from a single 2,3-DHB molecule (Feistner and Beaman 1987; Lopezgoni et al. 1992) to compounds such as vibriobactin, which consists of a norspermidine backbone, three catechol moieties, and two oxazoline rings (Griffiths et al. 1984).

Siderophores form very stable complexes with Fe^{3+} ions and show high specificity for Fe^{3+} over other environmentally prevalent metal ions (Crumbliss 1991; Dhungana and Crumbliss 2005); however, siderophores are very capable of binding other metals ions such as Ga^{3+}, Al^{3+}, Cr^{3+}, Pu^{4+}, and U^{+6} (Bouby et al. 1998; Evers et al. 1989; Gadd 1996; Neu et al. 2000). Siderophore–metal interactions may decrease metal mobility through microbial bioaccumulation or conversely, may enhance transport of metals via formation of bacterial colloids or soluble siderophore–metal complexes. Additionally, oxidation/reduction reactions, which can be mediated exclusively by the siderophore, or by the siderophore interaction at the cell surface or within the cell, may alter the metal oxidation state and the biogeochemistry of Fe (Dhungana and Crumbliss 2005). Thus, the effects of bacterial siderophores on metal mobility in the environment, particularly in the presence of organic contaminants, need to be further addressed.

Siderophore production by rhodococci, while noted, has been largely ignored with respect to structural and biochemical characterization. Heterobactins, a series of tetradentate mixed ligand siderophores produced by *Rhodococcus erythropolis* are the only siderophore characterized for rhodococci (Carrano et al. 2001). Rhodococci are known for their metabolic capabilities, particularly for their transformation of halogenated and aromatic pollutants (Warhurst and Fewson 1994). In particular, *Rhodococcus rhodochrous* has a broad degradative capacity. This organism can transform, and in some cases, use as a sole source of carbon and energy, toluene, anilines, and phenols (Fuchs et al. 1991; Karlson et al. 1993; Vanderberg et al. 2000). *Rhodococcus* spp. posses a number of additional traits that make them exceptionally well suited for bioremediation. For example, unlike *Pseudomonas* spp. and other Gram negative bacteria, *Rhodococci* do not exhibit catabolite repression (Warhurst and Fewson 1994). Also, many *Rhodococcus* spp. produce emulsifiers and flocculents that can aid in biodegradation of hydrocarbons and otherwise refractory organic pollutants (Finnerty 1992). These characteristics suggest that *Rhodococcus* spp. have the potential to be used broadly for bioremediation. As with all

microorganisms, in such an application its ability to thrive will depend on its ability to acquire iron. To better understand siderophore meditated iron transport, and to study the potential effect of siderophores on co-existing contaminant metals/radionuclides, we have purified and completely characterized a new siderophore produced by *R. rhodochrous* strain OFS. It is only fitting to call this newly characterized siderophore rhodobactin because it is produced by *Rhodococcus rhodochrous* and it contains two catecholate moieties for iron chelation.

Materials and methods

Bacterial strain and culture conditions

Rhodococcus rhodochrous strain OFS (ATCC 29672) was grown in iron-deficient minimal salts medium with 1.0% (v/v) hexadecane as sole source of carbon and energy. The medium was made from a 10× stock solution containing 2.0 g $(NH_4)_2SO_4$, 16.0 g NH_4Cl, 27.2 g KH_2PO_4, and 56.6 g $Na_2HPO_4{\cdot}7H_2O$ per liter (pH 6.8). The stock solution was passed through a chelex 100 resin (Sigma) column to remove all residual metals. Trace metals were added from a stock solutions: a 1000× fold stock of 97.7 g $MgSO_4$ per liter, and a 1000× trace element solution (70 mg $CuSO_4$, 35 mg $MnSO_4{\cdot}H_2O$, 23.7 mg $ZnCl_2$, 1000 mg $CaCl_2$, 18 mg $CoCl_2$, 7 mg H_3BO_3, and 60 mg $(NH_4)_6Mo_7O_{24}{\cdot}4H_2O$ per liter), and $FeSO_4{\cdot}7H_2O$to give a final Fe medium concentration of 1.0 μM. ^{15}N-labeled siderophore was generated by the replacement $^{14}NH_4Cl$ with $^{15}NH_4Cl$ in the 10× stock. To prepare the growth medium, stocks were diluted to 1× with deionized water (Milli-Q unit, Millipore Corp., Bedford, MA, water collected for use at 18 MΩ). Filter sterilized $FeSO_4$ solution and hexadecane were added to the media after autoclaving. All glassware (polycarbonate) was acid washed with concentrated nitric acid for a minimum of 1 h and rinsed repeatedly with deionized water.

AM-1 agar plates containing 10.0 μM Fe (as $FeSO_4$ solution) were streaked from a frozen culture of OFS. Then, 50 μl hexadecane was placed in the lid and the lid then placed on the streak plate. Following incubation, liquid cultures were inoculated with cells from these plates, grown to late log phase, and used as inoculum (2.0% of the growth medium volume). All iron-sensitive transfers were conducted using pyrogen-free/trace metal certified pipette tips (Fisher). Siderophore production was carried out by growing 2 l batch culture in 4 l acid washed conical flasks, at 30°C, in the dark, under constant shaking at 160 rpm for approximately 4 days.

Siderophore isolation and purification

Rhodobactin was isolated from the 4-day-old culture. Cells were removed from suspension by centrifugation at 10,000 rpm for 30 min at 4°C followed by filtration using polycarbonate 0.20-μm-pore-size filters. The crude culture extracts were concentrated by rotary evaporation and adjusted to pH 5 by the addition of 1% TFA. Rhodobactin was initially purified from the cell-free concentrated supernatant by preparative chromatography. The concentrated supernatant was passed through a chromatography column containing XAD-7 absorptive/partition resin (Sigma). The retained rhodobactin fraction was washed with 5 bed volumes of deionized water and sequentially eluted with an increasing percentage of methanol. Initially, the column was eluted with 10% methanol (1% TFA) until a steady baseline was obtained. Rhodobactin containing fractions were eluted off the column when the mobile phase contained 25% methanol (1% TFA). A UV absorption recorder set at 230 nm was used to record the chromatogram obtained during the elution. Siderophore-rich fractions were identified by UV–vis spectrophotometry, Arnow assay (Arnow 1937) and Chrome-azurol S assay (Schwyn and Neilands 1987). Crude siderophore was concentrated to dryness by rotary evaporation, suspended with a minimal amount of deionized water, and dried by lyophilization. Baseline separation of the rhodobactin from other remaining material by semi-preparative HPLC was achieved. The dried, semi-purified rhodobactin was a hygroscopic yellowish-white compound.

Semi-preparative HPLC

Rhodobactin was purified further using a Millipore Waters HPLC equipped with C_4 semi-preparative column and diode array detector set at 255 nm. An elution gradient of 99.9% water/0.1% trifluoroacetic acid (TFA) to 99.9% acetonitrile/0.1% TFA over 200 min was utilized. The peak corresponding to the siderophore was collected and dehydrated via lyophilization. Structural similarity between batches was confirmed by nuclear magnetic resonance spectroscopy (NMR) and electrospray ionization-mass spectrometry (ESI-MS).

Mass spectrometry

Mass spectrometric analyses was carried out using Q-Star quadrupole TOF mass spectrometer in positive ion mode (Applied Biosystems). All MS and CID MS/MS analyses were carried out using a NanoES Spray Capillaries (Protana Engineering A/S) mounted on the nanospray source (Proxeon, Denmark). The electrospray voltage was set at 1.8 kV. Rhodobactin sample used to inject into the ESI-MS was prepared in 30% Acetonitrile and 1% TFA.

NMR spectroscopy

All NMR spectra were collected at 298 K on a Bruker AVANCE 500 MHz instrument equipped with a triple resonance probe and triple axis gradients. All spectra were recorded using a ^{15}N-labeled sample of the siderophore dissolved in DMSO-d_6 and the solvent signal was used as internal reference for all ^{1}H and ^{13}C spectra; ^{15}N spectra were referenced to liquid ammonia (0.00 ppm) through the lock frequency. All spectra were processed and analyzed using XWINNMR software. The experimental details of the 1D and 2D NMR analysis are included in the supplementary materials and in our previous publication (Boukhalfa et al. 2006).

Siderophore hydrolysis

Purified rhodobactin was hydrolyzed to identify the position of the hydroxy groups on the catechol moieties. Pure rhodobactin was suspended in 6 N HCl, and refluxed at 100°C for 24 h. Rhodobactin hydrosylate was evaporated to dryness and suspended in triply distilled water. The catechol component of the siderophore was extracted at pH 2 with ethyl acetate and analyzed by ^{1}H-NMR and TLC using authentic 2,3-dihydroxybenzoic acid as a standard, using previously reported TLC conditions (Garner et al. 2004).

Siderophore assay and quantification

Catecholate siderophore levels were quantified using the Arnow assay (0.5 N HCl, 10 mg each of sodium nitrite and sodium molybdate in 100 ml water, and 1.0 M NaOH) (Arnow 1937). Catecholate positive material turned red (assay at 510 nm, see below). Samples were compared to a standard curve produced with purified siderophore to determine the concentration in solution.

Absorption spectroscopy

Optical absorption spectral analyses of the rhodobactin and Fe(III)-rhodobactin complexes were conducted using a Hewlett Packard 8453 spectrophotometer over a wavelength range of 210–500 nm. The Arnow colorimetric assay to detect catechol units within the siderophore structure uses the monitoring wavelength of 510 nm. The ligand:metal ratio for the siderophore binding Fe^{3+} was determined by acidifying purified rhodobactin solution to pH 3.8 and titrating the resulting solution with Fe(III) chloride. The adsorption band at 315 nm, corresponding to the catechol π–π^* transition, was monitored spectrophotometrically.

Metal binding

Stock solutions of Fe(III) chloride, plutonium (Pu)(IV) chloride, and uranium (U)(VI) nitrate were prepared for metal binding studies using optical absorbance and mass spectroscopies. A $FeCl_3$ stock solution was prepared by dissolving $FeCl_3$ in 0.1 M HCl and the final concentration of Fe was determined by using a graphite furnace atomic absorption spectrometry (GFAA). A

^{239}Pu stock solution was prepared and purified as previously described (Bond et al. 2000) and the solution purification used anion exchange chromatography. The stock solution was assayed by UV/vis spectroscopy to verify the Pu(IV) oxidation state purity and to determine the plutonium concentration. UV/vis/near-IR absorbance spectra for the Pu(IV) solution assay were obtained on a Cary 500 (Varian) spectrophotometer.

Fe uptake

A loopful of OFS was transferred from a plate to 200 ml of Fe-deficient medium in a 1 l shaker flask. Hexadecane (100 μl) was added as a carbon and energy source, and the culture was incubated with shaking for 24 h at 30°C. Cells were harvested by centrifugation and washed twice with 10.0 ml fresh Fe-deficient medium. Cells were re-suspended in fresh medium for uptake experiments. The dry-weight concentration of the cells was determined by drying a known volume of cell-suspension and subtracting the weight contribution of salts from uninoculated culture medium.

Fe(III)-complexes used in the uptake experiments were made by adding a known amount of Fe to an aqueous solution with a 5-fold excess of chelator. The unlabeled Fe stock solution was spiked with a small amount of the radioactive ^{55}Fe for quantification by liquid scintillation counting. Regular Fe was purchased as iron chloride, 1,000 ppm, in 2% HCl from Spex Certiprep, Inc. and ^{55}Fe was purchased as iron chloride in 0.5 M HCl from NEN Life Sciences Products, Inc.

Aliquots of washed cell suspensions (20 ml) were added to acid-washed 150 ml culture flasks at 22°C. Uptake was initiated by the addition of 2 μM Fe complexed with the purified rhodobactin, other siderophore (Rhodoturulic acid, ferrioxamine B) or small chelator (NTA, EDTA, Tiron) to the 20 ml cell suspensions. At selected time intervals, 1 ml aliquots were removed and the cells separated from the medium by filtration through 0.2 μm membranes (Poretics 25 mm PFTE membranes) using a Millipore 1225 Sampling Vacuum Manifold. The filters containing the cells were washed twice with 3 ml of a 5 mM EDTA, 333 mM NaCl solution.

Filters were removed from the filter membranes and added to scintillation cocktail (10 ml of Ultima Gold XR with. 2 ml water). ^{55}Fe concentrations were determined using a Wallac Guardian 1414 Liquid Scintillation Counter. To determine the correlation between counts per minute from the liquid scintillation counter and Fe concentration, 50 μl of the Fe-chelator solution before addition to the cell suspension, with a known concentration of Fe (including the spike of ^{55}Fe), was added to the cocktail and counted. Fe concentration on the filter was compared to the dry weight of OFS in 1 ml of medium. This yielded a value for uptake in pmol Fe per mg dry weight bacteria.

Results and discussion

Siderophore structure

The molecular mass of the siderophore produced by *R. rhodochrous*, rhodobactin, was obtained by ESI-MS analysis of the crude extracts and the purified siderophore obtained from cultures grown under iron-deficient conditions. The mass spectrum shows a molecular ion peak at m/z = 830 for the unlabeled siderophore and m/z = 840 for ^{15}N labeled siderophore. This suggested the presence of 10 nitrogen atoms in the molecule. The primary structure was determined using 1D and 2D ^{1}H, ^{13}C, and ^{15}N NMR studies and was confirmed by mass spectrometry fragmentation of rhodobactin obtained by ESI-MS CID analysis.

NMR analysis

^{1}H (Fig. 1), 13C and 15N (Fig. 2) NMR spectra of the ^{15}N-labeled rhodobactin were recorded to elucidate the primary structure of the compound. ^{15}N experiments confirmed the presence of 10 nitrogen atoms, four of which yield two strongly overlapped resonances and were deduced from integration of spectra. ^{15}N-DEPT experiments indicated that one of the nitrogen atoms (171.70 ppm) is tertiary (has no attached protons). The amide and amino protons of the siderophore were identified in the ^{1}H–^{15}N HSQC experiments and used as starting points for assignments. The amino acid side chains were

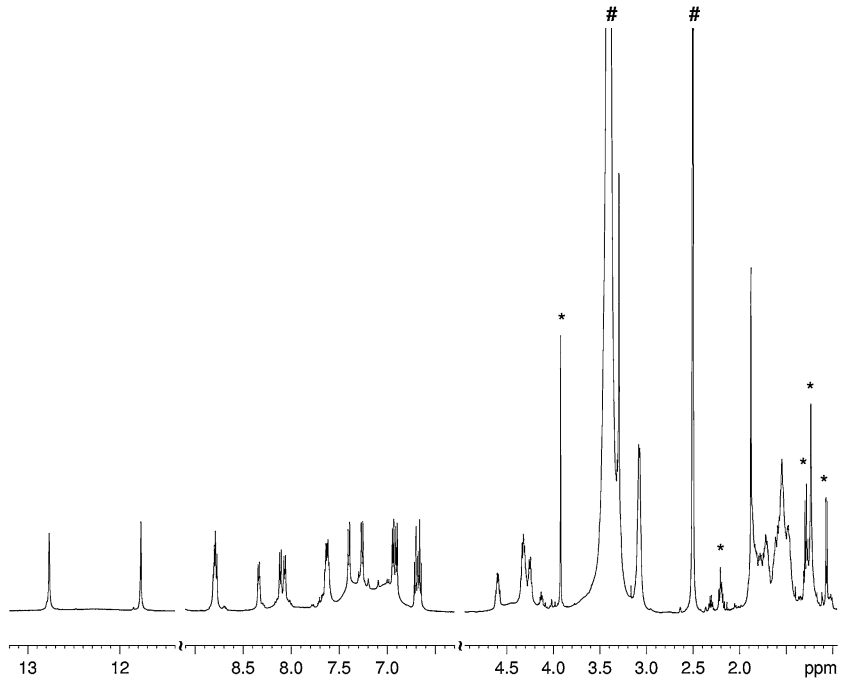

Fig. 1 ^{15}N-decoupled ^{1}H spectrum of ^{15}N-labeled RRS siderophore in DMSO-d_6. Residual solvent and water resonances are marked with #; peaks marked with asterisks (*) originate from impurities in the sample

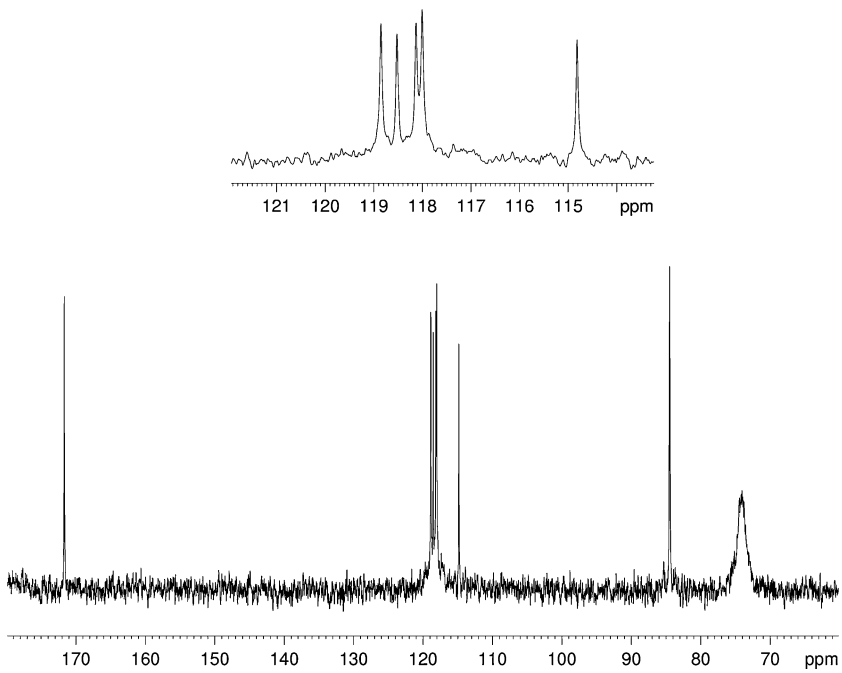

Fig. 2 ^{1}H-decoupled ^{15}N spectrum of RRS siderophore in DMSO-d_6. Inset shows the detail of the amide nitrogen region between 113 ppm and 122 ppm

subsequently assigned, beginning with NH protons, using a combination of ^{1}H–^{1}H DQF-COSY, NOESY and TOCSY spectra as well as ^{1}H–^{13}C and ^{1}H–^{15}N heteronuclear HSQC and LR-HSQC spectra.

The NOESY and TOCSY cross-peaks from αNH protons unambiguously yield positions of Hα and Hβ protons for each residue. Similarly, cross-peaks from εNH protons in TOCSY and NOESY spectra identify the Hδ proton resonance

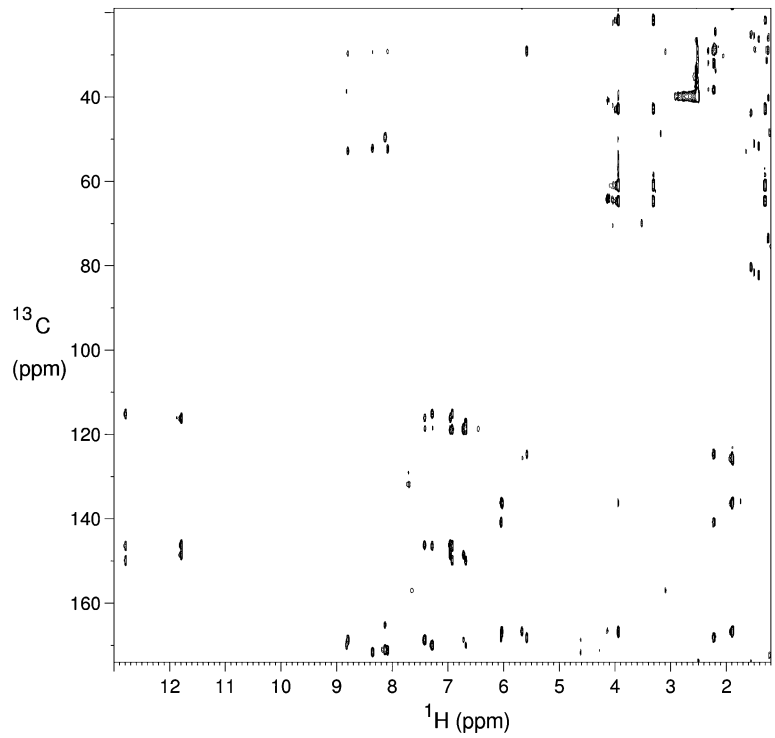

Fig. 3 ^{1}H–^{13}C long-range HSQC spectrum of the RRS siderophore showing multiple-bond C–H correlations, including correlations to carbonyl carbons. The direct one-bond correlations were not suppressed in the experiment

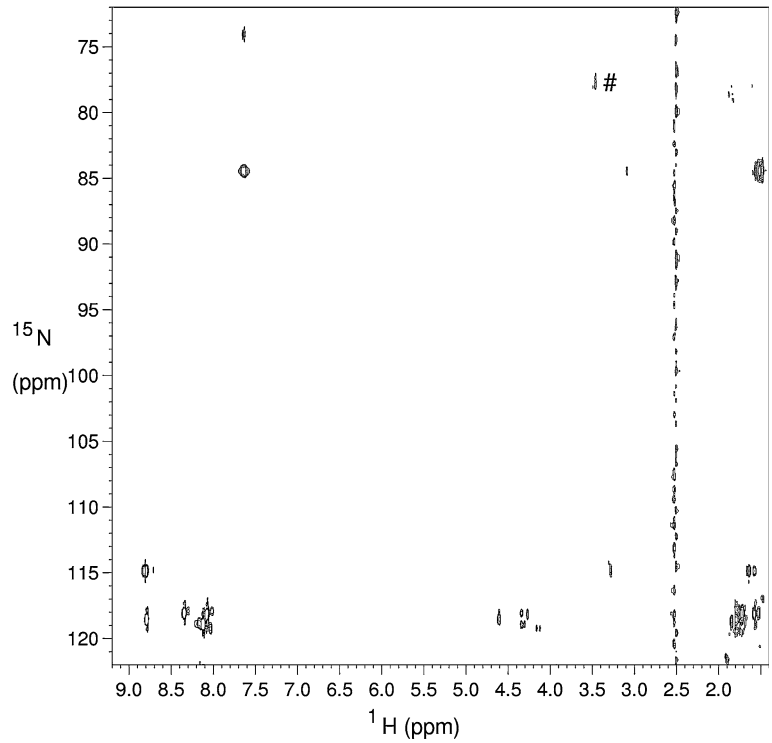

Fig. 4 ^{1}H–^{15}N long-range HSQC spectrum of the RRS siderophore showing multiple-bond N–H correlations. The direct one-bond correlations were not suppressed in the experiment. The cross-peak marked with # corresponds to the nitrogen resonance at 171.7 ppm and is folded twice in the ^{15}N dimension

positions. In the ^{1}H–^{13}C LR-HSQC spectra (Fig. 3) cross-peaks from αNH and εNH protons yield connectivities to Cα, Cβ and Cδ carbons. These assignments are confirmed by direct ^{1}H–^{13}C correlations in HSQC spectra. The Hγ and Cγ resonances were identified by cross-peaks

from Hα and Hδ protons in TOCSY and LR-HSQC spectra.

The tertiary nitrogen resonating at 171.70 ppm was assigned to the terminal AcOH-ornithine residue based on the two-bond correlation to the Hδ protons present in $^{1}H–^{15}N$ LR-HSQC spectrum (Fig. 4). The amino groups of the N-amido-ornithine residues yield very broad envelope in the proton spectrum and a broad resonance (overlapped) in the nitrogen spectrum. In the $^{1}H–^{15}N$ HSQC spectrum these nitrogens, at 84.15 and 83.99 ppm, exhibit weak correlations to protons at 7.45 and 6.95 ppm. The correlations are weak due to the magnetization losses during INEPT transfer of the HSQC experiment caused by large resonance line widths. The nitrogen resonances can be assigned to the amido NH_2 groups based on their three-bond correlation to the εNH protons in the $^{1}H–^{15}N$ LR-HSQC spectrum. Unfortunately, the amino nitrogens and protons do not exhibit any other cross-peaks and due to chemical shift degeneracy of εNH protons and nitrogens assignment of individual amino groups to either residue 3 or 4 was not possible. The εNH protons also exhibit a two-bond correlation to the carbonyl group in the side chain in the $^{1}H–^{13}C$ LR-HSQC spectrum and a cross-peak in the HNCO spectrum (Fig. 5), thus finalizing the assignments.

Two groups of proton and proton-bearing carbon resonances of the two catechols were easily identified in DQF-COSY, TOCSY and $^{1}H–^{13}C$ HSQC spectra. The remaining carbon resonances of the catechols, together with one hydroxyl proton resonance for each catechol, were identified from two- and three-bond couplings present in LR-HSQC. The other hydroxyl proton could not be identified in the spectra and is likely exchanging very fast with residual water in the sample and therefore resonates at the same frequency as water (strong resonance at ~3.3 ppm). The large downfield shift of the observed hydroxyl proton resonances (12.77 and 11.78 ppm) indicates that they are probably involved in hydrogen bonding, which slows down their exchange with solvent and also reduces the electron density around the protons thus shifting them downfield. Similarly, the carbonyl carbon

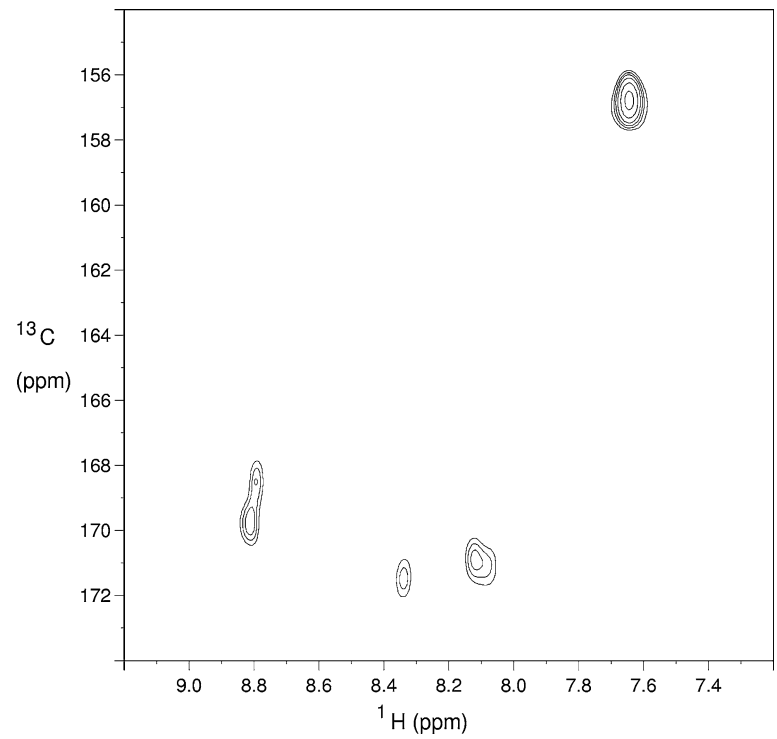

Fig. 5 M2D HNCO spectrum of the RRS siderophore showing through-bond correlations of amide protons to carbonyl carbons in the preceding residue

resonances of the catechol group were assigned from their long-range cross-peaks to H5 protons in LR-HSQC spectra.

Peptide chain sequence

Sequential assignments of the rhodobactin peptide chain were obtained from the combination of ^{1}H–^{1}H NOESY spectra, ^{1}H–^{13}C LR-HSQC and HNCO experiments. In the NOESY spectra, the cross-peak between H5 of the catechol A and the εNH resonance of ornithine 1 indicates that ornithine is bound directly to the catechol through its side chain nitrogen. Similarly, the NOESY cross-peak between H5 of the catechol B and the αNH resonance of ornithine 1 indicates that ornithine is bound directly to the catechol through its main chain nitrogen. These linkages are also confirmed by NH–CO cross-peaks, in the HNCO and ^{1}H–^{13}C LR-HSQC spectra, to previously identified catechol CO resonances. The presence of $NH_i \rightarrow H\alpha_i$ and $NH_i \rightarrow H\alpha_{i-1}$ cross-peaks was initially used to establish the connectivities between the neighboring residues. The connectivities were confirmed by the presence of $NH_i \rightarrow CO_{i-1}$ cross-peaks in the HNCO experiment, and the presence of $NH_i \rightarrow CO_{i-1}$ and $H\alpha_i \rightarrow CO_i$ cross-peaks in the LR-HSQC spectra.

The final assignments of ^{1}H, ^{13}C and ^{15}N resonances of rhodobactin are given in Tables 1–3. All chemical shifts fall in the range observed for similar groups in peptides and other siderophores. All 1D and 2D ^{1}H, ^{13}C and ^{15}N spectra not shown as figures in the manuscript are provided as supplementary material (Figs. S1–S5).

MS analysis

The amino acid sequence of rhodobactin obtained from NMR data is consistent with the fragment ions obtained by mass spectrometric analysis of both unlabeled and ^{15}N-labeled molecule (Table 4). The mass spectrum obtained by ESI-MS and ESI-MS/CID experiments showed a

Table 1 ^{1}H chemical shifts

	Hα	Hβ	Hγ	Hδ	NHα	NHε	NH_2
Ornithine 1	4.604	1.784	1.623	3.312	8.784	8.804	
			1.580				
N-amidoornithine 2	4.338	1.710	1.485	3.090	8.338	7.650	7.42/6.95[a]
		1.550					
N-amidoornithine 3	4.260	1.726	1.542	3.085	8.070	7.630	7.42/6.95[a]
		1.556					
AcOH-ornithine	4.322	1.840	1.867	3.469	8.113		
		1.610					
	H3	H4	H5	OH 1	OH 2		
Catechol A	6.902	6.666	7.269	12.77	ND		
Catechol B	6.940	6.703	7.407	11.78	ND		

[a] Due to the overlap of ^{15}N resonances of amino groups, ^{13}C resonances of Cζ and ^{1}H NHε resonances, residue specific assignments of amino groups could not be made

ND—not determined; OH resonances were not located in the spectra and most likely appear at the frequency of residual water in the solvent due to fast exchange; no cross-peaks were observed for these resonances

Table 2 ^{13}C chemical shifts

	Cα	Cβ	Cγ	Cδ	CO α	CO ζ	
Ornithine 1	52.68	29.57	25.59	38.54	171.48		
N-amidoornithine 2	52.01	29.33	24.89	40.44	170.97	156.77	
N-amidoornithine 3	52.22	29.13	24.70	40.40	170.83	156.79	
AcOH-ornithine	49.46	27.35	20.27	51.29	164.90		
	C1	C2	C3	C4	C5	C6	CO
Catechol A	149.65	146.22	118.49	117.89	117.10	114.97	169.75
Catechol B	148.33	146.05	118.76	118.20	118.38	116.00	168.48

Table 3 ^{15}N chemical shifts

	Nα	Nε	NH2	N–OH
Ornithine 1	118.54	114.83		
N-amidoornithine 2	118.03	84.83	74.15/73.99[a]	
N-amidoornithine 3	118.14	84.48	74.15/73.99[a]	
AcOH-ornithine	118.89			171.70

[a]Due to the overlap of ^{15}N resonances of amino groups, ^{13}C resonances of Cζ and ^{1}H NHε resonances, residue specific assignments of amino groups could not be made

molecular ion peak at m/z = 830.37 for the unlabeled rhodobactin and m/z = 840.25 for ^{15}N labeled rhodobactin, which is assigned to the parent molecule. The fragment peak observed at m/z = 693 and 557 are assigned to the cleavage of two catecholate groups (CatA and CatB) from the peptide chain. This is followed by a peak at m/z = 443, which results from the cleavage of amino acid ornithine (Orn1) responsible for holding the two catecholate groups together. The fragment peaks observed at m/z = 287 and 129 correspond to the cleavage of two N-amidoornithine (NamidoOrn2 and NamidoOrn3) groups and the peak corresponding to m/z = 129 is the AcOH-ornithine (AcOHOrn) fragment. The amino acid fragmentation pattern from the N-terminal fragments complemented the C-terminal fragmentation, this fragmentation data is summarized in Table 4. The ESI-MS CID data for the ^{15}N-labeled rhodobactin are also summarized in Table 4 and equivalent peaks in the ^{15}N-labeled rhodobactin are shifted to a higher mass depending upon the nitrogen content of the fragments. The distribution of the nitrogen atoms in the all the fragments is consistent with the NMR data. All ESI-MS spectra are provided as supplementary material (Figs. S7–S10).

Siderophore hydrolysis

The free catecholate groups resulting from the hydrolysis of purified rhodobactin were extracted with ethyl acetate at pH 2. The catechol component of rhodobactin had an R_f value and fluorescence on silica TLC identical to authentic 2,3-dihydroxybenzoic acid at both neutral pH and after ethyl acetate extraction at pH 2. ^{1}H NMR spectra of the aromatic region of the intact and hydrolyzed siderophore is identical to the ^{1}H NMR spectra of the aromatic region of the pure 2,3-dihydroxybenzoic acid (Supplementary Material Fig. S6). This confirmed the presence of 2,3-dihydroxybenzoic acid in rhodobactin.

The rhodobactin structure based on the NMR, ESI-MS and the acid hydrolysis data is shown in Fig. 6. Rhodobactin is a mixed ligand siderophore that consists of 1 hydroxamate and 2 catecholate groups for Fe(III) chelation. As this siderophore is produced by *Rhodococcus rhodochrous* strain OFS and it contains catecholate moieties for Fe(III) binding, it is only fitting to call this siderophore rhodobactin. The structure of rhodobactin is very similar to the structures of other mixed ligand siderophores produced by *Rhodococcus erythropolis* (Carrano et al. 2001).

Table 4 List of m/z for fragments of *R. rhodochrous* siderophore obtained by ESI-MS CID fragmentation and their assignments

Unlabeled (^{14}N) rhodobactin m/z	^{15}N-labeled rhodobactin m/z	C vs. N	Number of N in the fragment	Assignment of C and N-terminal fragments
137.01	137.01	B1	0	CatA-
387.13	389.06	B3	2	CatA-CatB-Orn-
543.22	548.24	B4	5	CatA-CatB-Orn-NamidoOrn1-
701.34 (350.67)[a]	709.21 (354.14)[a]	B5	8	CatA-CatB-Orn-NamidoOrn1-NamidoOrn2-
129.13	131.07	Y1	2	-AcOHOrn
287.20	292.13	Y2	5	-NamidoOrn2-AcOHOrn
443.29	451.20	Y3	8	-NamidoOrn1-NamidoOrn2-AcOHOrn
557.36	567.26	Y4	10	-Orn-NamidoOrn1-NamidoOrn2-AcOHOrn
693.37	703.26	Y5	10	-CatB-Orn-NamidoOrn1-NamidoOrn2-AcOHOrn
830.37	840.25		10	CatA-CatB-Orn-NamidoOrn1-NamidoOrn2-AcOHOrn

[a] Doubly charged peaks

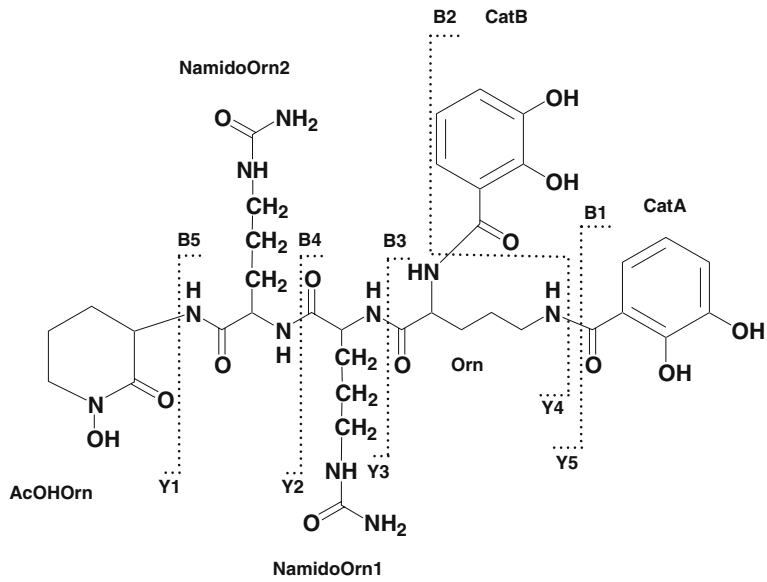

Fig. 6 Molecular structure of a rhodobactin, siderophore isolated from *R. rhodochrous* strain OFS (ATCC 29672). Bn and Yn refer to N-terminal and C-terminal fragments

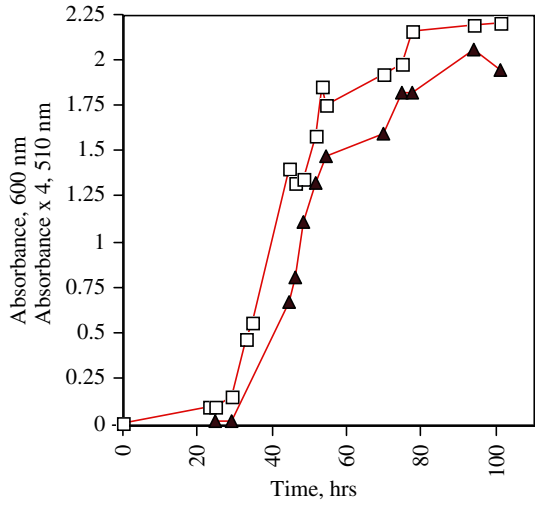

Fig. 7 Growth of *R. rhodochrous* OFS with 0.1% hexadecane as sole source of carbon and energy. Open squares, growth as measured by absorbance at 600 nm; closed triangles, siderophore production as monitored using the Arnow assay, measuring absorbance at 510 nm. Data shown are the average of duplicate determinations

Effect of Fe on siderophore production

Siderophore production by *Rhodococcus* species has been noted in the literature, but no purification or characterization of the Fe-binding systems had been undertaken until this study. As common to most bacterial siderophore systems, rhodobactin accumulated in solution almost simultaneously with cell growth (Fig. 7) (Chambers et al. 1996; Jadhav and Desai 1992). The concentration in solution decreased slightly at stationary phase (Fig. 7). The Fe concentration in the medium influenced the amount of Arnow positive material (Fig. 8) and cell mass-produced. Cultures utilizing chelexed AM-1 salts medium with no Fe present beyond the trace amounts in the medium, on the glassware, and in bacterial cell reserves yielded minimal cell growth and no detectable siderophore levels, demonstrating Fe starvation. *R. rhodochrous* cultures grown in non-chelexed medium with 0 μM added Fe produced siderophore at levels comparable to those grown in chelexed media with 110 μM added Fe, indicating the importance of chelex treatment of all media to remove any trace Fe when attempting to accurately determine the effects of Fe concentration on siderophore production. Siderophore production increased at Fe concentrations of 0.5 μM and reached a maximum concentration of 190 μM at 1.0 μM Fe. Dry weight cell mass of *R. rhodochrous* produced at Fe concentrations of 0, 0.1, 0.5, and 1.0 μM averaged 0.28, 0.67, 1.29, and 2.08 mg ml^{-1}, respectively. Cultures containing 2.0 μM Fe yielded an average of 100 μM Arnow-positive material. Production was repressed at Fe concentrations above 3.0 μM (Fig. 8).

Fe concentrations that yield maximum siderophore production (lower concentrations of Fe) or

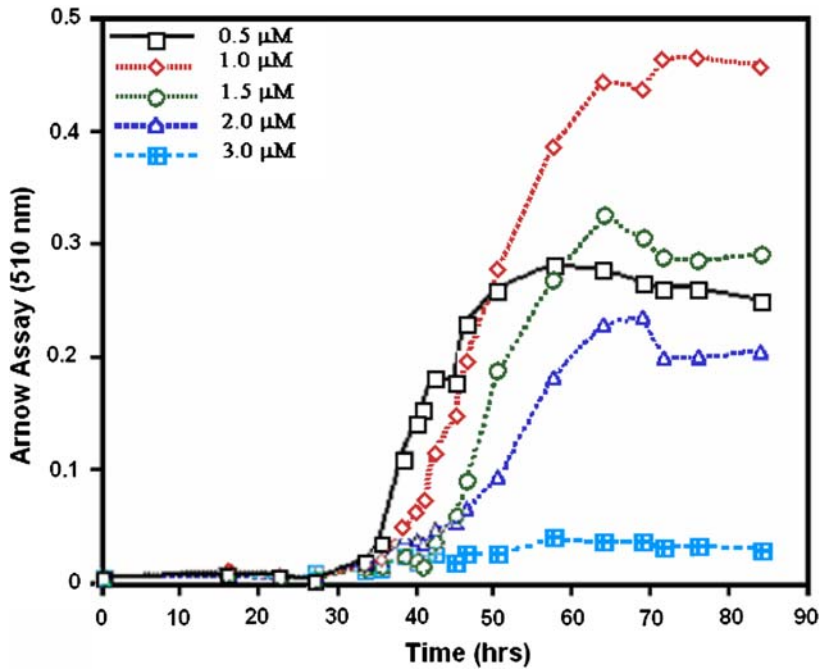

Fig. 8 Production of siderophore in cultures of *R. rhodochrous* OFS growing with 0.1% hexadecane. Iron was added from a separate stock solution and concentrations were varied. Relative concentration of siderophore was determined using the Arnow assay

that repress siderophore synthesis (higher concentrations of Fe) vary between bacterial strains and experimental techniques utilized, but siderophore production by *R. rhodochrous* followed a general trend. For example, Fe levels above 1.0 µM were found to repress siderophore production in *Staphylococcus aureus* (Heinrichs et al. 1999) and a *Rhizobium* strain isolated by Jadhav and Desai (1992) demonstrated maximum siderophore production at 1.0 µM with concentrations decreasing as levels approached 10.0 µM.

Siderophore was detected in supernatants of *R. rhodochrous* cultures containing 0.5 µM Fe before accumulation in 1.0 and 2.0 µM Fe cultures (Fig. 8). This lag in siderophore detection may be due to a regulatory response to the depletion of Fe in the medium, but was not investigated further.

Metal-binding

The π–π^* transition for catechols typically occurs at ~315 nm. This band was used to determine metal to ligand binding ratio for the purified rhodobactin. The experiments were conducted by addition of the metal to the ligand while maintaining a pH of 3.8. Titrating in (individually) Pu(IV) chloride, Fe(III) chloride, and U(VI) nitrate solutions resulted in a shift of the charge transfer band until a ratio of 1:1 was reached and no further change at greater ratios. Back titration with the disodium salt of EDTA, pH 3.8, showed

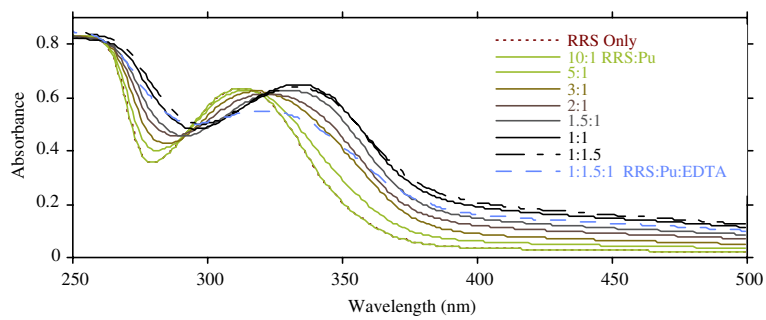

Fig. 9 UV/vis spectra of Pu(IV) titrated into a solution of the siderophore produced by *R. rhodochrous* and EDTA added to the resultant mixture

a broadening of the band; but at a ratio of 1:1 EDTA to siderophore (1.5 equiv. of Pu), the maximum absorbance band did not correlate with either unbound siderophore or with completely bound siderophore (Fig. 9). These data suggest that the binding strength of the siderophore is near the binding strength of EDTA, which has a formation constant with Pu(IV) of log β = 26.44 (Boukhalfa et al. 2004). The stoichiometry of the Fe (III) complex was also verified by obtaining mass spectra of the Fe-siderophore species.

Siderophore-mediated Fe uptake

Metabolically active cells of *R. rhodochrous* readily took up Fe-bound to its siderophore, whereas azide-inactivated cells and cells without a carbon source have reduced uptake, and heat killed cells have no iron uptake (Fig. 10). *R. rhodochrous* also internalized Fe bound to citrate and NTA chelators (NTA, Citrate), and showed to obtain iron from other chelators (EDDA, EDTA, Tiron, and possibly rhodotorulic acid), albeit at a much lower rate (data not shown).

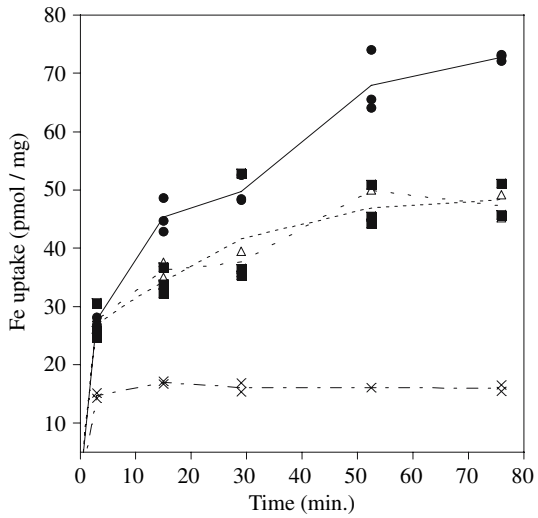

Fig. 10 Iron uptake by *R. rhodochrous* OFS. Cells were provided 0.1% hexadecane as sole source of carbon and energy and iron-bound siderophore. Experiments were performed as described in Materials and methods. - -●- - metabolically active cells; - -■- - no carbon source, - -△- - heat killed cells; - -×- - azide-inhibited cells; lines are the average of duplicate or triplicate determinations

Summary

Siderophore produced by *Rhodococcus rhodochrous* strain OFS, rhodobactin, was isolated and then purified by high performance liquid chromatography (HPLC) followed by drying to yield 15 mg per liter of a colorless solid. 1D and 2D ^{1}H, ^{13}C and ^{15}N NMR analysis were used to determine the structure of rhodobactin, which was further confirmed using ESI-MS CID analysis. The NMR analysis showed the presence of two nonequivalent catecholate and a hydroxamate moieties as the Fe(III) units in the siderophore. ESI-MS results showed the molecular weight of the isolated siderophore is 830 daltons.

The π–π* transition for catechols at ~315 nm was used to determine metal to ligand binding ratio for the purified rhodobactin. The experiments were conducted by the addition of the metal to the ligand while maintaining a pH of 3.8. These titration experiments showed that rhodobactin bound Fe(III) and U(VI) with 1:1 ratio, however the titration further indicated the binding ratio of rhodobactin to Pu(IV) was 1:1.5. These data also suggested the binding strength of rhodobactin is near the binding strength of the metal EDTA complex.

The uptake studies showed that Fe is taken up by the Gram positive *R. rhodochrous* strain OFS from its siderophore through an energy-dependent process, but this organism also showed to be capable of internalizing a variety of Fe(III)-complexes. *R. rhodochrous* is a common soil inhabitant that persists in the environment and can successfully scavenge Fe from a variety of sources. Given the broad metabolic capacity of this microbe and its Fe scavenging ability, *R. rhodochrous* OFS may have a competitive advantage over other organisms employed in bioremediation.

Acknowledgements This work was funded through a grant from the US Department of Energy, Office of Science, Office of Biological and Environmental Research, Natural and Accelerated Bioremediation Science Program (NABIR).

References

Albrecht-Gary A-M, Crumbliss AL (1998) Iron transport and storage in microorganism, plant, and animals. In: Sigel A, Sigel H (eds) Metal ions in biological systems. Marcel Dekker, New York, pp 239–328

Arnow LE (1937) Colorimetric determination of the components of 3,4-dihydroxyphenylalanine-tyrosine mixtures. J Biol Chem 118:531–537

Barbeau K, Zhang GP, Live DH, Butler A (2002) Petrobactin, a photoreactive siderophore produced by the oil-degrading marine bacterium *Marinobacter hydrocarbonoclasticus*. J Am Chem Soc 124:378–379

Barghouthi S, Young R, Olson MOJ, Arceneaux JEL, Clem LW, Byers BR (1989) Amonabactin, a novel tryptophan-containing or phenylalanine-containing phenolate siderophore in *Aeromonas-hydrophila*. J Bacteriol 171:1811–1816

Bond EM, Duesler EN, Paine RT, Neu MP, Matonic JH, Scott BL (2000) Synthesis and molecular structure of a plutonium(IV) coordination complex: [Pu(NO3)(2){2,6-[(C6H5)(2)P(O) CH2](2)C5H3NO}(2)](NO3)(2)·1.5H(2)O·0.5MeOH. Inorg Chem 39:4152–4155

Bouby M, Billard I, MacCordick J, Rossini I (1998) Complexation of uranium VI with the siderophore pyoverdine. Radiochim Acta 80:95–100

Boukhalfa H, Crumbliss AL (2002) Chemical aspects of siderophore mediated iron transport. Biometals 15:325–339

Boukhalfa H, Reilly SD, Michalczyk R, Iyer S, Neu MP (2006) Iron(III) coordination properties of a pyoverdin siderophore produced by *Pseudomonas putida* ATCC 33015. Inorg Chem 45:5607–5616

Boukhalfa H, Reilly SD, Smith WH, Neu MP (2004) EDTA and mixed–ligand complexes of tetravalent and trivalent plutonium. Inorg Chem 43:5816–5823

Carrano CJ, Jordan M, Drechsel H, Schmid DG, Winkelmann G (2001) Heterobactins: a new class of siderophores from *Rhodococcus erythropolis* IGTS8 containing both hydroxamate and catecholate donor groups. Biometals 14:119–125

Chambers CE, McIntyre DD, Mouck M, Sokol PA (1996) Physical and structural characterization of yersiniophore, a siderophore produced by clinical isolates of *Yersinia enterocolitica*. Biometals 9:157–167

Chipperfield JR, Ratledge C (2000) Salicylic acid is not a bacterial siderophore: a theoretical study. Biometals 13:165–168

Crichton RR (2001) Inorganic biochemistry of iron metabolism: from molecular mechanism to clinical consequences. Wiley, New York

Crumbliss AL (1991) Aqueous solution equilibrium and kinetic studies of iron siderophore and model siderophore complexes. In:Winkelmann G (ed) Handbook of microbial iron chelates. CRC Press, Boca Raton, FL, pp 177–233

Dhungana S, Crumbliss AL (2005) Coordination chemistry and redox processes in siderophore-mediated iron transport. Geomicrobiol J 22:87–98

Dhungana S, Miller MJ, Dong L, Ratledge C, Crumbliss AL (2003) Fe(III) coordination properties of an extracellular siderophore exochelin MN. J Am Chem Soc 125:7654–7663

Dong L, Miller MJ (2002) Total syntheses of exochelin MN and its analogs. J Org Chem 67:4759–4770

Evers A, Hancock RD, Martell AE, Motekaitis RJ (1989) Metal-ion recognition in ligands with negatively charged oxygen donor groups—complexation of Fe(Iii), Ga(Iii), in(Iii), Al(Iii), and other highly charged metal-ions. Inorg Chem 28:2189–2195

Feistner GJ, Beaman BL (1987) Characterization of 2,3-dihydroxybenzoic acid from *Nocardia-asteroides* Guh-2. J Bacteriol 169:3982–3987

Finnerty WR (1992) The biology and genetics of the genus *Rhodococcus*. Annu Rev Microbiol 46:193–218

Fuchs K, Schreiner A, Lingens F (1991) Degradation of 2-methylaniline and chlorinated isomers of 2-methylaniline by *Rhodococcus-rhodochrous* strain Ctm. J Gen Microbiol 137:2033–2039

Gadd GM (1996) Influence of microorganisms on the environmental fate of radionuclides. Endeavour 20:150–156

Garner BL, Arceneaux JE, Byers BR (2004) Temperature control of a 3,4-dihydroxybenzoate (protocatechuate)-based siderophore in *Bacillus anthracis*. Curr Microbiol 49:89–94

Griffiths GL, Sigel SP, Payne SM, Neilands JB (1984) Vibriobactin, a siderophore from *Vibrio-cholerae*. J Biol Chem 259:383–385

Guerinot ML (1994) Microbial iron transport. Annu Rev Microbiol 48:743–772

Hancock DK, Coxon B, Wang SY, White EV, Reeder DJ, Bellama JM (1993) L-threo-b-hydroxyhistidine, an unprecedented iron(III) binding amino acid in a pyoverdin type siderophore from *Pseudomonas fluorescens*. J Chem Soc Chem Commun 244:468–469

Heinrichs JH, Gatlin LE, Kunsch C, Choi GH, Hanson MS (1999) Identification and characterization of SirA, an iron-regulated protein from *Staphylococcus aureus*. J Bacteriol 181:1436–1443

Jadhav RS, Desai AJ (1992) Isolation and characterization of siderophore from cowpea Rhizobium (Peanut Isolate). Curr Microbiol 24:137–141

Karlson U, Dwyer DF, Hooper SW, Moore ERB, Timmis KN, Eltis LD (1993) 2 Independently regulated cytochromes-P-450 in a *Rhodococcus-rhodochrous* strain that degrades 2-ethoxyphenol and 4-methoxybenzoate. J Bacteriol 175:1467–1474

Koppisch AT, Browder CC, Moe AL, Shelley JT, Kinke BA et al (2005) Petrobactin is the primary siderophore synthesized by *Bacillus anthracis* str. Sterne under conditions of iron starvation. Biometals 18:577–585

Lopezgoni I, Moriyon I, Neilands JB (1992) Identification of 2,3-dihydroxybenzoic acid as a *Brucella-abortus* siderophore. Infect Immun 60:4496–4503

Neilands JB (1995) Siderophores: structure and function of microbial iron transport compounds. J Biol Chem 270:26723–26726

Neu MP, Matonic JH, Ruggiero CE, Scott BL (2000) Structural characterization of a plutonium(IV) siderophore complex: single-crystal structure of Pu-desferrioxamine E. Angew Chem Int Ed 39:1442–1444

Page WJ, Vontigerstrom M (1988) Aminochelin, a catecholamine siderophore produced by *Azotobacter-vinelandii*. J Gen Microbiol 134:453–460

Raymond KN, Telford JR (1995) Bioinorganic chemistry: an inorganic perspective of life. In: Kessissoglous DP (ed) NATO ASI series C, mathematical and physical sciences. Kluwer Academic Publishers, Dordrecht, The Netherlands, pp 25–37

Schwertmann U (1991) Solubility and dissolution of iron-oxides. Plant Soil 130:1–25

Schwyn B, Neilands JB (1987) Universal chemical-assay for the detection and determination of siderophores. Anal Biochem 160:47–56

Sharman GJ, Williams DH, Ewing DF, Ratledge C (1995) Determination of the structure of exochelin MN, the extracellular siderophore from *Mycobacterium neoaurum*. Chem Biol 2:553–561

Stintzi A, Raymond KN (2002) Siderophore chemistry. In: Templeton DM (ed) Molecular and cellular iron transport. Marcel Dekker, Inc., New York, pp 273–320

Vanderberg LA, Krieger-Grumbine R, Taylor MN (2000) Evidence for diverse oxidations in the catabolism of toluene by *Rhodococcus rhodochrous* strain OFS. Appl Microbiol Biotechnol 53:447–452

Warhurst AM, Fewson CA (1994) Biotransformations catalyzed by the genus Rhodococcus. Crit Rev Biotechnol 14:29–73

Winkelmann G (1991) Handbook of microbial iron chelates. CRC Press, Boca Raton, FL

Yamamoto S, Okujo N, Fujita Y, Saito M, Yoshida T, Shinoda S (1993) Structures of 2 polyamine containing catecholate siderophores from *Vibrio-fluvialis*. J Biochem 113:538–544